Strength and elastic moduli of TiN from radial x-ray diffraction under nonhydrostatic compression up to 45 GPa

Haihua Chen,[1] Fang Peng,[1,a)] Ho-kwang Mao,[2,3] Guoyin Shen,[2,3] Hanns-Peter Liermann,[2,3] Zuo Li,[1] and Jinfu Shu[2]
[1]*Institute of Atomic and Molecular Physics, Sichuan University, Chengdu 610065, China*
[2]*Geophysical Laboratory, Carnegie Institution of Washington, Washington, District of Columbia 20015,USA*
[3]*HPCAT, Carnegie Institution of Washington, Argonne, Illinois 60439, USA*

(Received 16 December 2009; accepted 18 March 2010; published online 1 June 2010)

The high pressure behavior of titanium nitride (TiN) was investigated using synchrotron radial x-ray diffraction (RXRD) under nonhydrostatic compression up to 45.4 GPa in a diamond-anvil cell. We obtained the hydrostatic compression equation of state of TiN. Fitting to the third-order Birch–Murnaghan equation of state, the bulk modulus derived from nonhydrostatic compression data varies from 232 to 353 GPa, depending on angle ψ, the orientation of the diffraction planes with respect to the loading axis. The RXRD data obtained at $\psi=54.7°$ yield a bulk modulus $K_0=282\pm9$ GPa with pressure derivative K_0' fixed at 4. We have analyzed the deformation mechanisms by analyzing the (111), (200), (220), (311), and (222) peaks in the x-ray diffraction under pressures. The ratio of uniaxial stress component to shear modulus t/G ranges from 0.007–0.027 at the pressure of 6.4–45.4 GPa. It was found that the TiN sample could support a maximum uniaxial stress component t of 8.6 GPa, when it started to yield at 45.4 GPa under uniaxial compression. And the aggregate elastic moduli of TiN at high pressure were determined from the synchrotron RXRD measurements. © *2010 American Institute of Physics*. [doi:10.1063/1.3392848]

I. INTRODUCTION

Titanium nitride (TiN) as a new type of metal compound coating material with unique combination properties aroused great research interests. Such as good corrosion resistance, good wear resistance, high melting point, high toughness, high thermal conductivity, and high electrical conductivity.[1–3] These superior properties have made TiN widely used in various industrial applications. TiN belongs to a class of so called refractory metals compounds.[4] At ambient pressure, TiN keeps an NaCl-type structure like other refractory transition metal nitrides.[5]

Recently, much interest has been inspired on investigating the behavior of materials under extreme pressures by using diamond-anvil cell (DAC), especially using the radial x-ray diffraction (RXRD) experiments in DAC. The advantages of such RXRD experiments are that, the information of materials can be obtained from different spatial directions. The elasticity and plastic deformation effects as well as the hydrostatic equation of state can be obtained from the highly nonhydrostatic compression data under high pressures. Although, there are large number of experiments devoted to various aspects of TiN film growth[3,6,7] and many theoretical calculations about elastic modulus for TiN,[4,8] direct experimental measurements of elastic properties, strength, and plastic deformation behavior are rare. However, Zhao *et al.*[9] investigated the behavior of TiN using axial x-ray diffraction under high pressure to 30.1 GPa. Their experimental results suggested an isostructural phase transition at about 7 GPa as shown by the discontinuity of V/V_0 data with pressure. The purpose of this study is to investigate the equation of state and stress state of TiN in a DAC under uniaxial stress conditions with the synchrotron RXRD,[10–13] Together with the lattice strain theory,[12–16] we also determined the aggregate moduli of TiN at high pressure from the RXRD measurements.

II. EXPERIMENT

A panoramic DAC with a culet size of 300 μm was used in the experiment. TiN powder (Alfa, 99.7%) was loaded into 50 μm diameter hole of a boron gasket which made of a boron–epoxy central disk of 400 μm diameter surrounded by a Kapton® (DuPont) confining ring 120 μm thick.[17] A piece of ~15 μm Pt was placed on top within 20 μm of the sample center and served as a pressure standard[18] as well as a position reference for the RXRD measurement. No pressure-transmitting medium was used. Energy-dispersive RXRD experiments[13,16] were performed at the high-pressure collaborative access team (HPCAT), beamline 16-BMB of the advanced photon source, Chicago, USA. The diffracted intensity was recorded using a Ge solid-state detector with a fixed angle at $2\theta=12.0°$. The incident x-ray beam was focused by a pair of Kirkpatrick–Baez mirrors to approximately 7×10 μm^2 and directed through the boron gasket and the sample. The DAC was mounted in a rotation stage whose axis bisects 2θ. The RXRD patterns were taken at $\psi=0°$, 15°, 30°, 54.7°, 60°, 75°, and 90°, respectively. The ψ is the angle between the diffraction plane normal and the cell-loading axis. Before data collection, the cell was scanned in the horizontal and vertical directions while recording x-ray transmission with a photodiode to make sure that the incident x-ray beam goes through the sample center.

a)Author to whom correspondence should be addressed. Electronic mail: pengfang8888@yahoo.com.cn.

 © 2010 American Institute of Physics

Downloaded 19 Aug 2010 to 164.54.164.42. Redistribution subject to AIP license or copyright; see http://jap.aip.org/about/rights_and_permissions

At each pressure load, RXRD patterns were taken at different angles and the pressures were determined from the lattice parameter of Pt. For the TiN sample, the analysis was based on the diffraction lines of (111), (200), (220), (311), and (222).

III. THEORY

Lattice strains theory at the center of the compressed specimen in a DAC under nonhydrostatic pressure conditions has been described elsewhere.[15,16,19,20] Here, we present a short summary of the main features. The stress tensor in the center of a diamond cell sample can be expressed as

$$\sigma = \begin{bmatrix} \sigma_1 & 0 & 0 \\ 0 & \sigma_1 & 0 \\ 0 & 0 & \sigma_3 \end{bmatrix} = \begin{bmatrix} \sigma_p & 0 & 0 \\ 0 & \sigma_p & 0 \\ 0 & 0 & \sigma_p \end{bmatrix} + \begin{bmatrix} -t/3 & 0 & 0 \\ 0 & -t/3 & 0 \\ 0 & 0 & 2t/3 \end{bmatrix}, \quad (1)$$

where σ_1 and σ_3 are the radial and axial stress components, respectively. σ_p is the mean normal stress (or equivalent hydrostatic pressure). The difference between the σ_1 and σ_3 is the uniaxial stress component t, which is taken to be positive on compression,

$$t = \sigma_3 - \sigma_1 \leq 2\tau = Y, \quad (2)$$

where τ is the shear strength and Y is the yield strength of the material. Actually, t could be less than the yield strength before the sample is yielded.[19]

The equation for the d spacing measured by x-ray diffraction is given by following relation:

$$d_m(hkl) = d_p(hkl)[1 + (1 - 3\cos^2\psi)Q(hkl)], \quad (3)$$

where $d_m(hkl)$ is the measured d spacing and $d_p(hkl)$ is the d spacing under the hydrostatic pressure, $Q(hkl)$ is given by

$$Q(hkl) = (t/3)\{\alpha[2G_R(hkl)]^{-1} + (1-\alpha)(2G_V)^{-1}\}. \quad (4)$$

$G_R(hkl)$ and $G_V(hkl)$ are the shear moduli of the aggregate under the Reuss (isostress) and Voigt (isostrain) approximations, respectively, and are not orientation dependent. The parameter α, which varies between 0 and 1, specifies the degree of stress and strain continuity across grains in the sample.

For the cubic system,

$$(2G_R)^{-1} = S_{11} - S_{12} - 3S\Gamma(hkl), \quad (5)$$

where S, a measure of the elastic anisotropy, is given by

$$S = S_{11} - S_{22} - S_{44}/2, \quad (6)$$

and

$$\Gamma(hkl) = (h^2k^2 + k^2l^2 + h^2l^2)/(h^2 + k^2 + l^2)^2 \quad (7)$$

and

$$(2G_v)^{-1} = \{(5/2)[(S_{11} - S_{12})S_{44}]\}/[3(S_{11} - S_{22}) + S_{44}], \quad (8)$$

where the Sij are the single-crystal elastic compliances.

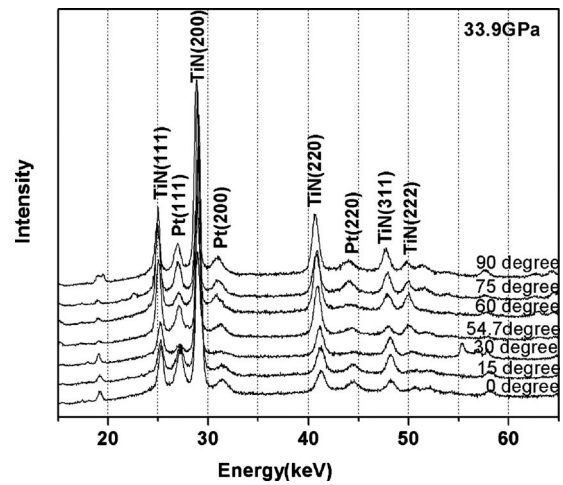

FIG. 1. X-ray diffraction patterns of the TiN sample taken at different angles under the same loading. The pressure is determined from the lattice parameter of Pt observed at $\psi = 54.7°$.

According to Eq. (3), $d_m(hkl)$ should vary linearly with $1-3\cos^2\psi$. The $d_p(hkl)$ can be directly measured at $\psi = 54.7°$ (namely $1-3\cos^2\psi = 0$). The slope of the $d_m(hkl)$ versus $1-3\cos^2\psi$ relation yields the product $d_p(hkl)Q(hkl)$.

Equations (4)–(6) indicate a linear relationship between $Q(hkl)$ and $\Gamma(hkl)$ with slope m_1 and intercept m_0 given by

$$m_0 = (t/3)[S_{11} - S_{22}], \quad (9)$$

$$m_1 = -(t/3)[S_{11} - S_{22} - S_{44}/2], \quad (10)$$

for the case where $\alpha = 1$.

The linear compressibility χ of a cubic crystal is given by

$$\chi = -(\partial \ln a/\partial p)_T = 1/3K = S_{11} + 2S_{22}, \quad (11)$$

where a is the lattice parameter and K is the isothermal bulk modulus.

According to Eq. (4), the uniaxial stress component t can be estimated using the relation[16,19,20]

$$t = 6G\langle Q(hkl)\rangle, \quad (12)$$

where $\langle Q(hkl)\rangle$ represents the average $Q(hkl)$ value over all observed reflections, and G is the aggregate shear modulus of the polycrystalline sample. If the uniaxial stress component t has reached its limiting value of yield strength at high pressures, $t/G = 6\langle Q(hkl)\rangle$ will reflect the ratio of yield strength to shear modulus.[21] We can deduce the three elastic compliances S_{11}, S_{22}, and S_{44} of a cubic material using above information, and can invert the three independent elastic stiffnesses C_{11}, C_{12}, and C_{44}.[20]

IV. RESULTS AND DISCUSSION

Figure 1 shows the RXRD patterns of the TiN sample at different ψ, which are measured under the conditions corresponding to a hydrostatic pressure of 33.9 GPa at room temperature. It can be seen that diffraction peaks always shift to smaller energy as ψ increased, reflecting that increase in strain as the diffraction plane normal approaches the maximum stress axis. Here the pressure is determined using the Pt

Downloaded 19 Aug 2010 to 164.54.164.42. Redistribution subject to AIP license or copyright; see http://jap.aip.org/about/rights_and_permissions

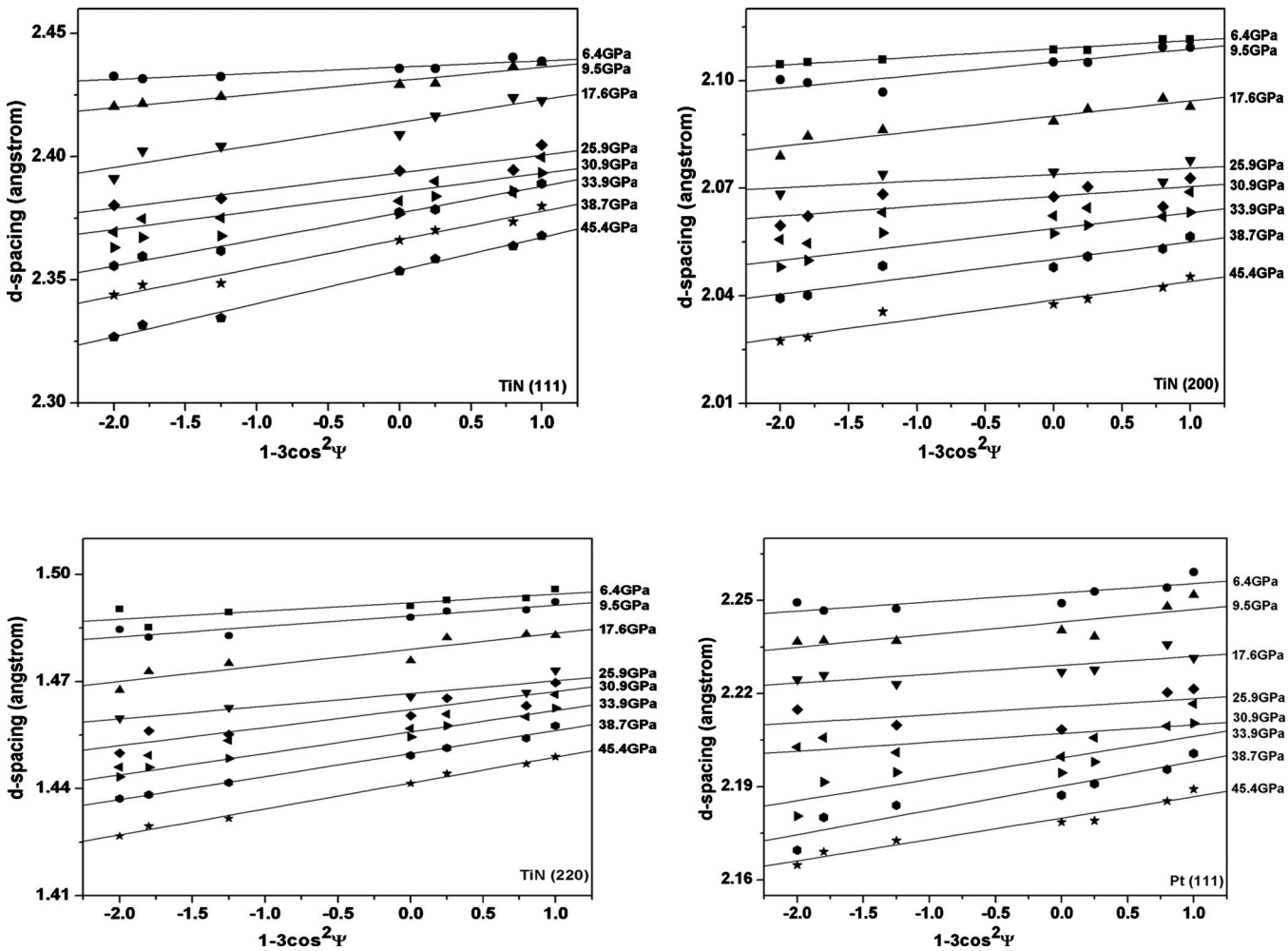

FIG. 2. Dependence of observed d spacing on $1-3\cos^2\psi$ for selected diffraction lines of TiN and Pt at different pressure. The pressure are determined from the lattice parameter of Pt obtained at $\psi=54.7°$. The pressures are listed to the right of each line.

scale[18] from the RXRD data obtained at $\psi=54.7°$. Based on the lattice strain theory,[15,16,19,20] the observed d spacing at $\psi=54.7°$ equals to the d spacing under hydrostatic compression of the sample. Therefore, the hydrostatic compression curve can be directly derived from the diffraction data at $\psi=54.7°$.

The d spacing as a function of $1-3\cos^2\psi$ for selected diffraction lines of TiN and Pt at different pressures are shown in Fig. 2. As expected from the theory, for both TiN and Pt, the measured d spacing varies linearly with $1-3\cos^2\psi$. As shown in the Fig. 2, the d spacing increases with the ψ increasing from $\psi=0°$ to 90°. It indicates that the uniaxial stress component reaches a maximum at $\psi=0°$, then the uniaxial stress component drops off with the ψ increasing and reaches a minimum at $\psi=90°$. The values of $Q(hkl)$ for different diffraction planes can be obtained by the slope of the $d_m(hkl)$ versus $1-3\cos^2\psi$ at different pressures.

The compression curves derived from our experiments vary smoothly with pressure increasing at different angles ($\psi=0°$, 54.7°, and 90°) are shown in Fig. 3. The variation in the relative volume V/V_0 (V_0 is the unit-cell volume at zero pressure, V is the volume at nonzero pressure) with direction is caused by the uniaxial stress component t, which is limited by the yield strength of material. The unit-cell volumes observed at different pressures were fitted to the third-order Birch–Murnaghan equation of state (EOS). The bulk modulus K_0 obtained at $\psi=54.7°$ is 282 ± 9 GPa with K_0' fixed at 4, which corresponds to the hydrostatic compression curve.[11,13,16] Therefore, the hydrostatic compression curve

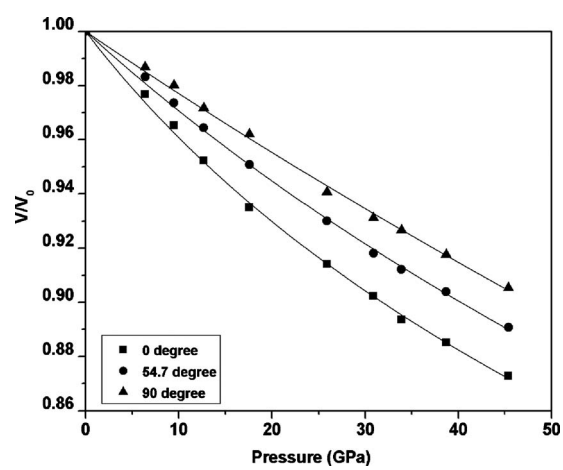

FIG. 3. Compression curves of TiN from lattice parameters measured at $\psi=0°$, 54.7°, and 90° under different pressures. The pressure is determined from the lattice parameter of Pt at each direction. The solid lines are the Birch–Murnaghan equation fits to the data.

Downloaded 19 Aug 2010 to 164.54.164.42. Redistribution subject to AIP license or copyright; see http://jap.aip.org/about/rights_and_permissions

TABLE I. A summary of the bulk modulus and its pressure derivative of TiN in this work and others methods.

Method	K_0 (GPa)	K_0'	Reference
RXRD	282 ± 9	4 (fixed)	This work
Experiment	288		Ref. 21
Acoustic microscope	320		Ref. 22
GGA	282	4.2	Ref. 4
Ab initio calculation	390		Ref. 23

can be obtained from highly nonhydrostatic data by choosing proper angle between the stress axis and the diffraction vector. Table I summarizes the bulk modulus and its pressure derivative of TiN from previous experiments and theoretical calculations. Our value for bulk modulus is in very good agreement with the experimental value from Gubanov *et al.*[21] and the theoretical value obtained by generalized gradient approximation implemented density functional theory (GGA-DFT).[4] Our RXRD value of the bulk modulus is less than the acoustic microscope values. The differences may be caused by the different experimental method and also in the different nature of the samples used. The bulk moduli obtained from fits using the third-order Birch–Murnaghan EOS at maximum stress direction $\psi=0°$ and minimum stress direction $\psi=90°$ are 232 ± 14 GPa and 353 ± 19 GPa, respectively.

The dependence of $Q(hkl)$ on $3\Gamma(hkl)$ at pressure P =45.4 GPa is shown in Fig. 4. For TiN, a linear relationship is observed. It confirms the linear relationship between $Q(hkl)$ and $3\Gamma(hkl)$ indicated by theory. The aggregate shear modulus G and Young's modulus E are derived from the Cij at high pressure.[24] If we know the shear modulus G, we can obtain uniaxial stress component t of TiN using Eq. (12) at each pressure step. The ratio of uniaxial stress component t to shear modulus t/G for TiN is shown in Fig. 5. It varies from 0.007–0.027 in the pressure range of 6.4–45.4 GPa. The change of t/G with pressure may predicate that the TiN starts yielding, and t reaches its limiting value at a nonhydrostatic compression of ~18 GPa, which means that the TiN sample begins to yield at about 18 GPa. The value of

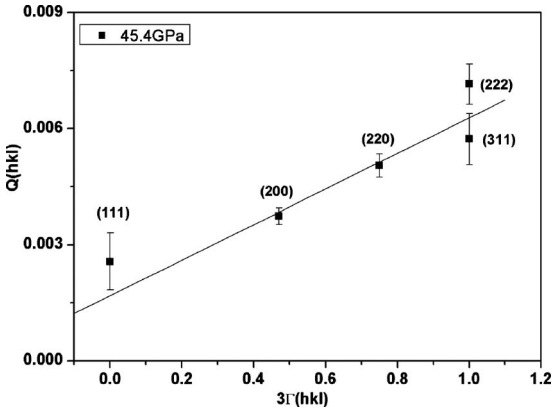

FIG. 4. $Q(hkl)$ as a function of $3\Gamma(hkl)$ for TiN at maximum pressure 45.4 GPa. The estimated errors on $Q(hkl)$ are derived from the scatter of the $d_m(hkl)$ vs $1-3\cos^2\psi$ relation.

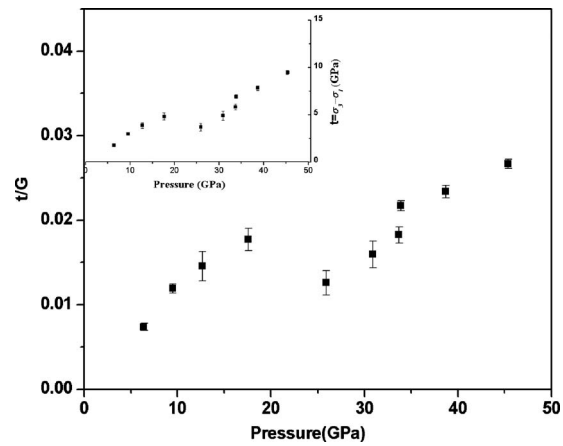

FIG. 5. Ratio of uniaxial stress component t to shear modulus G for TiN sample. The estimated errors are obtained from the scatter of $d(hkl)$ vs $1-3\cos^2\psi$.

t/G can be directly obtained from the average slope of the d spacing versus $1-3\cos^2\psi$ relation.[11,19,20] As TiN sample has deformed plastically, the uniaxial stress component t is equivalent to the yield strength, and the t/G reflects the ratio of yield strength to shear modulus.[11] The value of yield strength reaches the highest value 8.6 GPa at the highest pressure 45.4 GPa. It is larger than those stiff pure metals, such as molybdenum[20] and tungsten,[24] which are investigated using RXRD under high pressure. However, compared with the strong solid materials SiC[25] and Al_2O_3,[26] the yield strength of TiN is less than them. The SiC started to yield at ~14 GPa, and the yield strength is 13.6 GPa by analyzing the diffraction peak broadening under nonhydrostatic compression.[25] The yield strength of Al_2O_3 reaches a maximum of 12 GPa at perssure 70 GPa.[26] It appears that the measured t/G above the yield point could reflect the hardness for the strong materials under nonhydrostatic compression.[24]

Figure 6 shows that the aggregate elastic moduli of TiN vary with the pressures. Using the third-order Birch–Murnaghan equation, the bulk modulus are directly derived from the RXRD measurements at $\psi=54.7°$. The aggregate

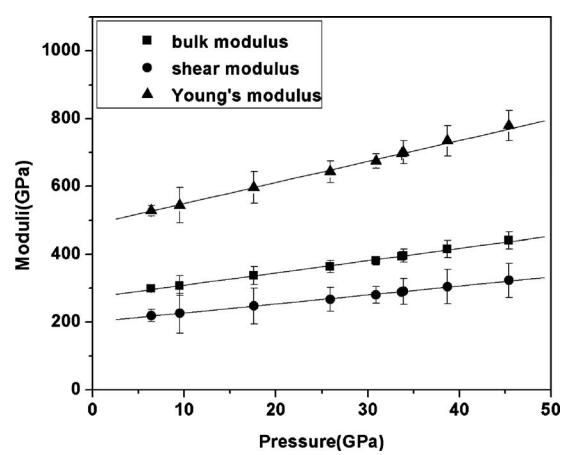

FIG. 6. Values of aggregate moduli calculated from RXRD measurements for TiN sample at high pressure. The solid triangles, squares, and circles express the aggregate Young's modulus, bulk modulus, and shear modulus, respectively.

Downloaded 19 Aug 2010 to 164.54.164.42. Redistribution subject to AIP license or copyright; see http://jap.aip.org/about/rights_and_permissions

Young's modulus E and shear modulus G can be deduced from the intrinsic relationship. As shown in Fig. 6, the three moduli all increase with the augmentation of the pressure. The solid triangles, squares, and circles express the aggregate Young's modulus, bulk modulus, and shear modulus, respectively. The solid lines are the linear fitting. From the linear fitting, the slope and intercept of TiN are known. Therefore, we can obtain the normal equation of the aggregate elastic moduli for TiN, as follows:

$$B = 275.4 + 3.5\ \mathrm{P}, \tag{13}$$

$$G = 202.3 + 2.5\ \mathrm{P}, \tag{14}$$

$$E = 487.7 + 6.2\ \mathrm{P}, \tag{15}$$

where B, G, and E are the bulk modulus, shear modulus, and Young's modulus, respectively.

V. CONCLUSION

In summary, the elastic and plastic properties of TiN are systematically studied using synchrotron RXRD measurements together with the lattice strain theory in our study. The hydrostatic compression curve can be obtained from highly nonhydrostatic data by choosing proper angle between the stress axis and the diffraction vector by RXRD technique. The hydrostatic component has been obtained at $\psi = 54.7°$, which yields a bulk modulus $K_0 = 282 \pm 9$ GPa with its pressure derivative K_0' fixed at 4. Our result is in good agreement with experimental value from Ref. 21 and the theoretical calculation value.[4] The agreement between results obtained in our study and those obtained with other methods demonstrates that the reliability of the technique in our experiment. The yield strength of TiN sample obtained in this work reaches the highest value 8.6 GPa at the highest pressure 45.4 GPa under uniaxial compression. It appears that the measured t/G reflects the hardness for the strong materials above the yield point under nonhydrostatic compression. The yield strength of TiN is considerably larger than those reported strong materials such as molybdenum and tungsten at static high pressure. Moreover, by analyzing the nonhydrostatic compression data, we obtained the aggregate elastic moduli as the functions of pressure.

ACKNOWLEDGMENTS

We thank names of beamline scientists who supported the experiments for experimental assistance. HPCAT is supported by DOE-BES, DOE-NNSA, NSF, and the W. M. Keck Foundation. APS is supported by DOE-BES, under Contract No. DE-AC02-06CH11357.

[1] A. Kobayashi, Surf. Coat. Technol. **132**, 152 (2000).
[2] J. P. Tu, Corros. Sci. **42**, 147 (2000).
[3] J. B. Price, J. O. Borland, and S. Selbrede, Thin Solid Films **236**, 311 (1993).
[4] M. Marlo and V. Milman, Phys. Rev. B **62**, 2899 (2000).
[5] R. Chauhan, S. Singh, and R. K. Singh, Cent. Eur. J. Phys. **6**, 277 (2008).
[6] R. I. Hegde, R. W. Fiordalice, E. O. Travis, and P. J. Tobin, J. Vac. Sci. Technol. B **11**, 1287 (1993).
[7] U. C. Oh and J. H. Je, J. Appl. Phys. **74**, 1692 (1993).
[8] R. Ahuja, O. Eriksson, J. M. Wills, and B. Johansson, Phys. Rev. B **53**, 3072 (1996).
[9] J. G. Zhao, L. X. Yang, Y. Yu, S. J. You, R. C. Yu, F. Y. Li, L. C. Chen, C. Q. Jin, X. D. Li, Y. C. Li, and J. Liu, Chin. Phys. Lett. **22**, 5 (2005).
[10] T. S. Duffy, G. Shen, D. L. Heinz, J. Shu, Y. Ma, H. K. Mao, R. J. Hemley, and A. K. Singh, Phys. Rev. B **60**, 15063 (1999).
[11] D. W. He, S. R. Shieh, and T. S. Duffy, Phys. Rev. B **70**, 184121 (2004).
[12] T. S. Duffy, G. Shen, J. Shu, H. K. Mao, R. J. Hemley, and A. K. Singh, J. Appl. Phys. **86**, 6729 (1999).
[13] S. R. Shieh, T. S. Duffy, and B. S. Li, Phys. Rev. Lett. **89**, 255507 (2002).
[14] A. K. Singh, J. Appl. Phys. **73**, 4278 (1993).
[15] A. K. Singh, J. Appl. Phys. **74**, 5920 (1993).
[16] A. K. Singh, H. K. Mao, J. Shu, and R. J. Hemley, Phys. Rev. Lett. **80**, 2157 (1998).
[17] S. Merkel and T. Yagi, Rev. Sci. Instrum. **76**, 046109 (2005).
[18] V. N. Antonov, V. Yu. Milman, V. V. Nemoshkalenko, and A. V. Zhalko-Titarenko, Z. Phys. B: Condens. Matter **79**, 233 (1990).
[19] S. Merkel, A. P. Jephcoat, J. Shu, H.-K. Mao, P. Gillet, and R. J. Hemley, Phys. Chem. Miner. **29**, 1 (2002).
[20] A. K. Singh, C. Balasingh, H.-K. Mao, R. J. Hemley, and J. F. Shu, J. Appl. Phys. **83**, 7567 (1998).
[21] V. A. Gubanov, A. L. Ivanovsky, and V. P. Zhukov, *Electronic Structure of Refractory Carbides and Nitrides* (Cambridge University Press, Cambridge, 1994).
[22] J. O. Kim, J. D. Achenbach, P. B. Mirkarimi, M. Shinn, and S. A. Barnett, J. Appl. Phys. **72**, 1805 (1992).
[23] V. P. Zhukov, V. A. Gubanov, O. Jepsen, N. E. Christensen, and O. K. Andersen, J. Phys. Chem. Solids **49**, 841 (1988).
[24] D. W. He and T. S. Duffy, Phys. Rev. B **73**, 134106 (2006).
[25] J. Zhang, L. Wang, D. J. Weidner, T. Uchida, and J. Xu, Am. Mineral. **87**, 1005 (2002).
[26] C. Meade and R. Jeanloz, Phys. Rev. B **42**, 2532 (1990).

Downloaded 19 Aug 2010 to 164.54.164.42. Redistribution subject to AIP license or copyright; see http://jap.aip.org/about/rights_and_permissions